Review of Scientific Instruments

Combination of pulsed light heating thermoreflectance and laser-heated diamond anvil cell for *in-situ* high pressure-temperature thermal diffusivity measurements

Cite as: Rev. Sci. Instrum. **90**, 074901 (2019); https://doi.org/10.1063/1.5093343
Submitted: 20 February 2019 • Accepted: 15 June 2019 • Published Online: 10 July 2019

Akira Hasegawa, Takashi Yagi and Kenji Ohta

Review of Scientific Instruments ARTICLE scitation.org/journal/rsi

Combination of pulsed light heating thermoreflectance and laser-heated diamond anvil cell for *in-situ* high pressure-temperature thermal diffusivity measurements

Cite as: Rev. Sci. Instrum. 90, 074901 (2019); doi: 10.1063/1.5093343
Submitted: 20 February 2019 • Accepted: 15 June 2019 •
Published Online: 10 July 2019

Akira Hasegawa,[1,2] Takashi Yagi,[1,a)] and Kenji Ohta[2]

AFFILIATIONS

[1]National Metrology Institute of Japan, National Institute of Advanced Industrial Science and Technology, Tsukuba, Ibaraki 305-8563, Japan
[2]Department of Earth and Planetary Sciences, Tokyo Institute of Technology, Meguro, Tokyo 152-8551, Japan

[a)]**Author to whom correspondence should be addressed:** t-yagi@aist.go.jp

ABSTRACT

By combining thermoreflectance measurements and laser heated diamond anvil cell (LHDAC) techniques, an instrument for the measurement of *in situ* high pressure-temperature thermal diffusivity of materials was developed. In an LHDAC system, high-power continuous-wave laser beams irradiate both faces of a disk-shaped metal sample loaded into diamond anvil cells (DACs), to maintain a stable high-temperature condition. During the operation of the LHDAC system, temperature of the sample is determined from the thermal radiation spectrum between 640 and 740 nm to fit Planck's law. Subsequently, a pulsed laser beam irradiates the metal disk to induce a temperature gradient inside the sample, and the transient temperature, caused by heat diffusion, is measured by a continuous wave probe laser based on the thermoreflectance phenomenon. We determined the thermal conductivities of Pt and Fe up to approximately 60 GPa and 2000 K using the measured thermal diffusivities and obtained values consistent with previous works. The uncertainties in the pressure and the temperature are estimated to be approximately 10%, and that in the thermal conductivity is estimated to approximately 15%. The system developed in this study enables us to determine thermal transport properties of materials under pressure–temperature conditions of the deep Earth.

I. INTRODUCTION

The thermal transport properties of the Earth's constituents are important in understanding the thermal evolution and the heat budget of the Earth.[1] To determine terrestrial heat flux, a large amount of data on thermal conductivity of a variety of crust rocks has been reported.[2–6] High pressure apparatus has been combined with thermal conductivity measurement systems to investigate the thermal transport properties of the mantle and the core materials. The Ångstrom method has been employed for samples in large volume presses to constrain pressure and temperature responses of thermal diffusivity and conductivity of various mantle minerals and their polymorphs and analogs.[7–12] A pulse heating method 脉冲加热 was also combined with the high-pressure apparatus, which is applicable not only to measurement of materials with anisotropic thermal conduction but also to obtain information on heat capacity under high pressure.[13] However, these techniques have been limited to a maximum of 26 GPa and 1273 K, similar to the conditions in the uppermost part of the lower mantle.[12]

The diamond anvil cell (DAC) can reach pressure-temperature conditions comparable to those in the deeper Earth and is compatible with laser optical techniques. A laser flash-heating method in a DAC succeeded in extracting the thermal conductivity of materials at pressures and temperatures of the Earth's core.[14–20] However, the pumped pulsed laser produces temperature disturbances in the DAC sample of more than a few hundred kelvin, which leads to

values of the thermal conductivity with large uncertainty. For instance, Konôpková *et al.*[20] determined the thermal conductivity of iron at 130 GPa and 2525 ± 725 K.

A time domain thermoreflectance (TR) method has been also applied to a DAC, to measure the thermal diffusivity of condensed materials[21,22] to constrain their thermal conductivity. The TR method utilizes a temperature coefficient of the reflectivity of metals, typically of 10^{-4} to 10^{-5} K^{-1}, as a sensor of sample temperature. A metal coated mineral or a bare metal in a DAC is heated by a laser pulse to induce a very small heat flow, and the temporal temperature of the sample can be measured from the intensity of another probe laser beam irradiated at the sample. The TR method has the following advantages when applied to a DAC technique:

(1) The time resolution of the temporal temperature measurement is fast enough for a very thin sample in the DAC, which depends on the heating laser pulse duration and the reflectivity measurement response.
(2) The positions of TR measurement and the heating in the sample are locally selectable, by manipulating both laser spots.
(3) The temperature increase from a pulse heating is less than 10 K, typically a few kelvins, so the disturbance in a steady temperature condition is generally negligible.
(4) They are easily combined with other optical systems, such as radiation measurements and laser heating.

With the TR combined with the DAC method, we successfully measured the thermal diffusivities of the Earth's lower mantle minerals, reaching pressure conditions equal to those in the Earth's core-mantle boundary (135 GPa) but at room temperature.[23,24] To extend the measurable temperature range, the TR method may be combined with a laser-heated DAC (LHDAC) technique, which is able to generate the pressure-temperature conditions present in the center of the Earth.[25]

In this study, we developed a new instrument to measure the thermal diffusivity of metal samples *in situ* at high pressures and temperatures based on the combination of the TR method and the LHDAC system. To evaluate the performance of the developed system, we carried out high pressure-temperature thermal diffusivity measurements on Pt and Fe up to 1914 K, which yielded values consistent with previous studies.[18,20]

II. INSTRUMENTATION

For the LHDAC system, high power continuous wave (CW) laser beams irradiated both faces of a disk-shaped sample to maintain a steady state temperature (Fig. 1). During operation of the LHDAC system, a pulsed laser beam (TR pump laser) irradiated the sample to induce a temperature gradient inside the sample. To measure the transient temperature, caused by heat diffusion from the heated face to the opposite face, we irradiate the opposite face of the sample with a CW probe laser (TR probe laser) beam to detect reflectivity changes due to the temperature change in the sample (i.e., thermoreflectance,[26] TR).

The optical design of our apparatus is shown in Fig. 2. The TR pump laser is a pulsed fiber laser with a wavelength of 1064 nm, pulse width of 1 ns, pulse frequency of 50 kHz, and averaged power of 15 mW (0.3 μJ/pulse). The TR pump laser beam is focused by an

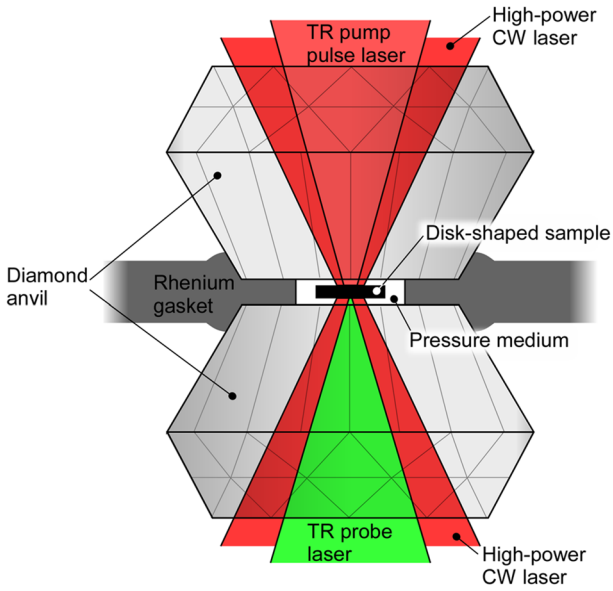

FIG. 1. Schematic of the cross section of the DAC and the arrangement of four laser beams for the TR pump laser, TR probe laser, and heating CW laser.

objective lens with a power of 20 (Nikon, LR Plan APO NIR), which are parfocal correction at wavelengths of 532 and 1064 nm. The typical spot size of the TR pump laser is 25–30 μm in diameter, which can be scanned on the sample surface using a scan mirror and a scan lens. The TR probe laser is a linearly polarized CW laser with a wavelength of 532 nm and averaged power of 40 mW. An incident TR probe laser beam with a vertical polarization state is reflected by a polarized beam splitter (PBS) and then converted to a circular polarized beam by a $\lambda/4$ waveplate. The TR probe laser beams is focused by the same type of objective lens as used for the TR pump laser. The typical spot size is less than 5 μm in diameter. The reflected TR probe laser beam is converted to a horizontal polarization state by the $\lambda/4$ waveplate and passes through the PBS. The intensity of the reflected TR probe laser was detected by using a high-speed photodetector with a bandwidth of 1.4 GHz. A notch filter with an optical density of 6 at 1064 nm positioned in front of the detector eliminates scattered TR pump and LHDAC laser light. The measured transient temperature signal is averaged by an oscilloscope with a 2 GHz bandwidth.

A linearly polarized CW fiber laser (KKFL-20, KIMMON KOHA) with a wavelength of 1064 nm and a maximum output power of 20 W is used to generate a steady-state high-temperature condition in the sample. The transverse mode of the laser is a Gaussian beam. The laser beam is divided by a half mirror. One laser beam is coaxially combined with the TR pump laser beam using a PBS. The other is also coaxially combined with the TR probe laser beam using a harmonic separator, which can reflect 1064 nm light and transmit 532 nm light. Both high-power CW laser beams are focused by the objective lens with a typical diameter of 25–30 μm. The focus images of those four laser spots at the sample surface are observed by using digital cameras (Nikon D3400, from which we

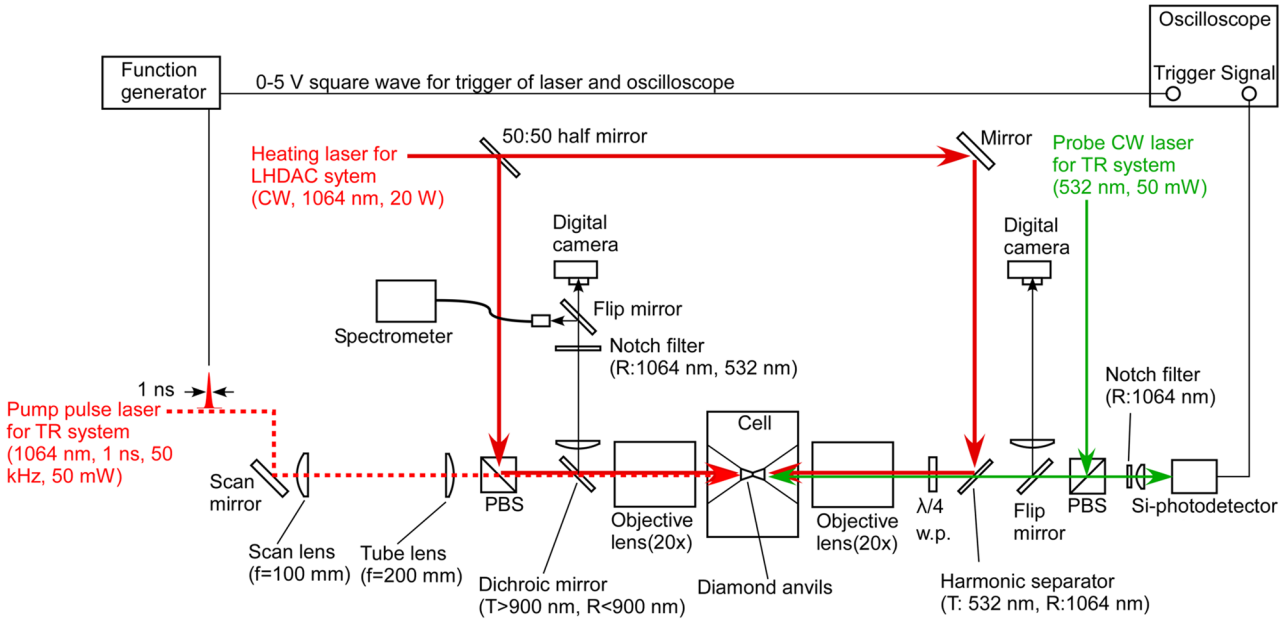

FIG. 2. Thermal conductivity measurement system at high pressure and high temperature condition with a coaxial double beam path of thermoreflectance laser beams (green lines and dashed red lines) and laser heating DAC laser beams (solid red lines).

removed an IR cut filter in front of the CMOS) positioned on both sides of the DAC.

The temperature of the sample during the LHDAC operation is determined from the thermal radiation spectrum to fit Planck's law. The thermal radiation emitted from the heated sample is collected through the objective lens and reflected by a dichroic mirror. A double notch filter for 1064 and 532 nm wavelengths is positioned in front of the spectrometer to eliminate scattered laser light from the thermal radiation. Finally, a thermal radiation spectrum between 640 and 740 nm is collected by the spectrometer. The losses from the optical system for each wavelength are calibrated using a halogen lamp.

III. RESULTS AND DISCUSSION

A. Test measurements of thermal diffusivities of Pt and Fe at high pressures and temperatures

To demonstrate the effectiveness of the apparatus, we measured the high-temperature thermal diffusivity of Pt and Fe at high pressures. High pressure conditions were generated in a symmetric-type DAC with 300 μm flat culet diamond anvils. The samples were a Pt foil (99.98% purity) and an Fe foil (99.99% purity) with an initial thickness of 20 μm. The foils were cut into disk shapes with a diameter of approximately 100 μm and were loaded in the DAC, along with a pressure medium. NaCl and/or sapphire disks were used as pressure media. A Re foil was used as a gasket. After assembling the DAC, the sample was compressed, and the attained pressure was measured by the Raman shift of the diamond anvil.[27] Figure 3 shows photographs and a schematic illustration of the Fe sample loaded in the DAC, with the beam spots of the TR probe laser (532 nm), TR pump laser (1064 nm), and LHDAC laser (1064 nm).

The thermal diffusivity (α) is a function of heat diffusion time through the sample (τ) and the sample thickness (d), which can be converted to the thermal conductivity (κ) using the density (ρ) and the isobaric heat capacity (C_P),

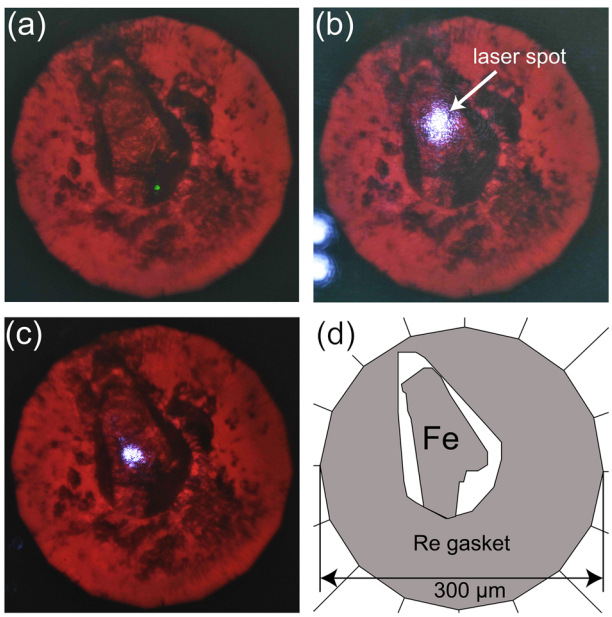

FIG. 3. Photographs and schematic of the sample inside the DAC. Image of the sample with the (a) TR probe laser spot, (b) TR pump laser spot, (c) heating CW laser spot of the LHDAC system, and (d) schematic illustration of the DAC sample.

$$\alpha = \frac{d^2}{\tau}, \tag{1}$$

$$\kappa = \rho C_P \alpha. \tag{2}$$

Therefore, we measured τ at high pressure-temperature conditions from the TR measurement with the LHDAC and then determined d from observation of the recovered sample. To convert from the thermal diffusivity to the thermal conductivity, the values of ρ and C_P at high-pressure and high-temperature conditions were also estimated on the basis of the Debye approximation and the equation of state (EOS) of Pt[28] and Fe.[29,30] Under high-temperature conditions, the pressure change owing to thermal expansion was estimated from the thermal equation of state of Pt[28] and Fe.[30]

First, we performed two separate runs for Pt at 40.0 and 55.6 GPa, up to 1914 K (Table I). Figures 4(a) and 4(b) show the obtained thermal radiation spectra for the Pt sample at high-temperature conditions generated by the LHDAC laser. Representative transient temperature signals for the Pt sample, measured at room temperature and high-temperature conditions, are shown in Fig. 5(a). These curves represent heat diffusion of the disk-shaped sample from the heated face to the opposite face after 1 ns TR pump laser irradiation, as well as heat effusion from the sample to the pressure medium. We analyzed the measured curves based on a one-dimensional heat conduction model, assuming that a planar sample was embedded between semi-infinite pressure media. According to the model, the transient temperature can be represented as follows:[22]

$$T(t) = \overline{T}\sqrt{\frac{\tau}{\pi t}}\sum_{n=0}^{\infty}\gamma^{2n}\exp\left[-\frac{(2n+1)^2}{4}\frac{\tau}{t}\right], \tag{3}$$

where $T(t)$ is the temperature, $\overline{T}$ is a constant, t is time, and $\gamma = (b_m - b_p)/(b_m + b_p)$ is related to heat effusion from the sample to the pressure medium, where b_m and b_p are the thermal effusivity (J/(m^2 s$^{0.5}$ K)) of the metal sample and the pressure medium, respectively. During the high temperature measurements, there is a huge temperature gradient inside the pressure media, which may lead to inhomogeneity in b_p. Therefore, the longer time region data far from τ were ignored for the analysis. We took into account n from 0 to 7th terms in Eq. (3). At 40–43 GPa and 300 K, 1315 K, and 1914 K, we obtained heat diffusion times τ of 219 ns, 211 ns, and 152 ns, respectively. Our results indicate that temperature enhances the heat diffusion of Pt. After the TR measurements with the LHDAC, we recovered the Pt sample and prepared its cross section using a focused ion beam (FIB) apparatus and then observed it under a scanning electron microscope (SEM). The observed sample thickness was at ambient conditions; hence, d at the high pressure was corrected using the equation of state of Pt.[28] In the same manner as the first run, we also carried out the thermal conductivity measurement on Pt at 55.6 GPa. The obtained thermal conductivity of Pt is summarized in Fig. 7(a) along with values obtained in previous studies.[18,31] The thermal conductivity of Pt at 40–42 GPa increases by 16% as the temperature increases from 300 to 1315 K. This behavior is very similar to that obtained in the ambient pressure

TABLE I. Experimental pressures (P), temperatures (T), heat diffusion times (τ), sample thicknesses (d), thermal diffusivity (α), densities (ρ), isobaric heat capacities (C_P), and thermal conductivities (κ) of Pt and Fe.

Run	Sample	P (GPa)	T (K)[a]	τ (ns)	d (μm)[b]	α (mm^2/s)	ρ (kg/m^3)[c]	C_P (J/(kg K))[d]	κ (W/m K)
1	Pt	40.0(40)	300	181.3(18)	2.40(15)	32.3(43)	23 976	123.2	95.3(126)
		40.0(40)	300	236.0(24)	2.68(15)	30.4(37)	23 976	123.2	89.7(109)
		40.0(40)	300	219.3(22)	2.68(15)	32.7(37)	23 976	123.2	96.6(111)
		42.0(42)	1315(132)	210.6(21)	2.69(15)	34.4(40)	23 873	136.0	111.7(128)
		42.0(42)	1317(132)	229.0(23)	2.69(13)	31.6(34)	23 871	136.2	102.8(112)
		42.7(43)	1699(170)	167.3(17)	2.42(15)	35.0(48)	23 835	139.0	115.8(158)
		43.0(43)	1837(184)	152.1(15)	2.42(15)	38.4(52)	23 822	140.0	128.3(173)
		43.2(43)	1914(191)	152.4(15)	2.42(15)	38.4(51)	23 815	140.6	128.5(172)
2	Pt	55.6(56)	300	51.5(17)	1.40(14)	38.2(75)	24 741	121.9	115.2(228)
		57.7(58)	1266(127)	56.5(11)	1.40(14)	34.9(68)	24 645	134.2	115.4(226)
		58.2(58)	1531(153)	55.5(10)	1.41(14)	35.6(70)	24 620	135.8	118.9(233)
		58.3(58)	1565(157)	52.4(10)	1.41(14)	37.7(74)	24 620	136.0	126.1(247)
3	Fe	49.8(50)	300	2256(28)	6.56(39)	19.1(25)	9 923	421.9	80.0(104)
		52.8(53)	1259(126)	3938(157)	6.58(39)	11.0(17)	9 848	510.5	55.3(87)
		53.0(53)	1346(135)	4168(72)	6.58(39)	10.4(14)	9 842	529.0	54.1(73)
		53.2(53)	1385(139)	5398(153)	6.58(39)	8.0(12)	9 839	537.5	42.4(62)
		53.2(53)	1400(140)	5579(211)	6.58(39)	7.8(12)	9 837	540.7	41.3(64)
		53.3(53)	1423(142)	4838(97)	6.58(39)	9.0(12)	9 835	545.7	48.1(66)
		53.4(53)	1449(145)	5653(199)	6.58(39)	7.7(12)	9 833	551.2	41.5(63)

[a] Fixed error at 10%.
[b] After correction for pressure effects using P-V-T EOSs of Pt[27] and Fe.[29]
[c] Calculated from P-V-T EOSs of Pt[27] and Fe.[29]
[d] Calculated from P-V-T EOSs of Pt[27] and Fe[28,29] and Debye approximation.

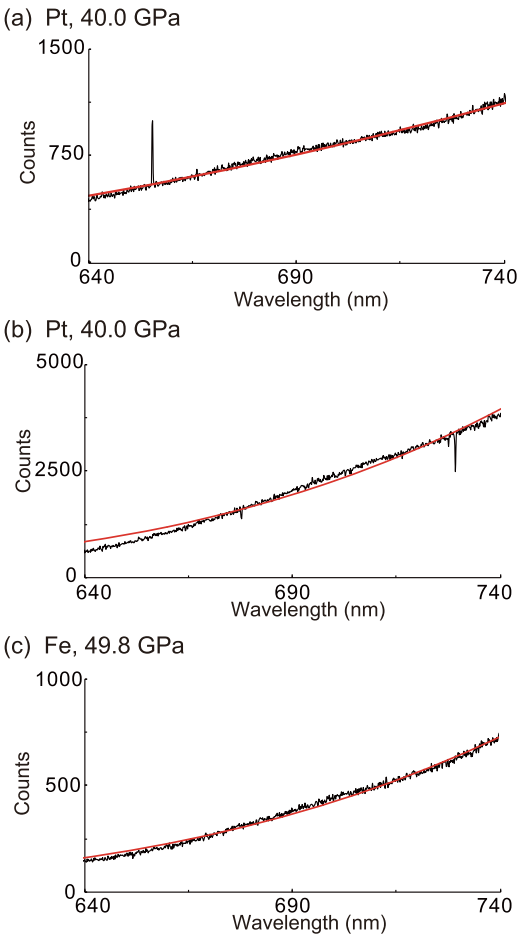

FIG. 4. Thermal radiation spectra of (a) and (b) Pt and (c) Fe samples during laser heating. The red lines are the fitted result based on Planck's law. The determined temperatures were 1315 ± 132 K and 1914 ± 191 K for Pt and 1346 ± 135 K for Fe. The uncertainty estimation of temperature is shown in Sec. III B.

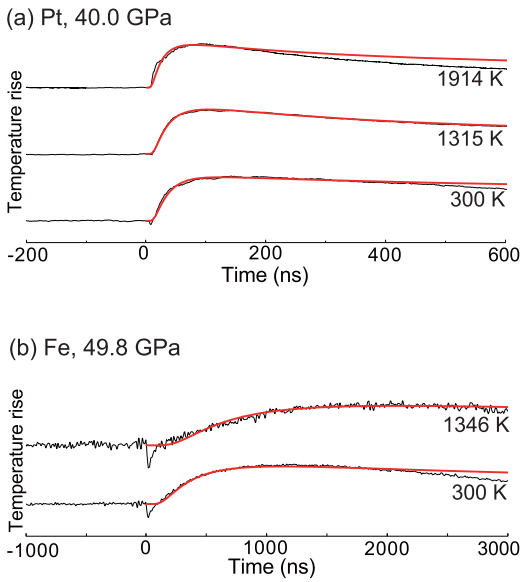

FIG. 5. Representative transient temperature signals for (a) Pt and (b) Fe at 300 K and higher temperatures. The black line is the measured signal, and the red line is the fitted result based on Eq. (3).

condition.[31] Our data at 43.2 GPa and 1914 K are in good agreement with previous measurements.[18] Since Pt films are commonly used as a reflective layer in TR methods with DAC,[22,23] our data are useful for further experiments on not only metals but also oxides and silicate minerals at high pressure-temperature conditions.

The thermal transport properties of Fe are of great importance to study the thermal evolution and the dynamics of the Earth's core, but there is no consensus yet.[20,32] We carried out a pilot experiment to determine the thermal conductivity of Fe at 49.8 GPa up to 1449 K, using our new instrument [Table I, Fig. 4(c)]. The Fe sample shows a hexagonal close-packed (hcp) phase in the experimental pressure-temperature conditions.[33] From the obtained TR signals for Fe [Fig. 5(b)], we confirmed that its heat diffusion time increased with increasing temperature, in contrast with the results for Pt. The sample thickness d was determined from the recovered sample (Fig. 6) considering the effects of lattice volume expansion due to decompression and transformation from hcp to bcc phase using the EOS of hcp iron.[30] Figure 7(b) shows the temperature dependence of the thermal conductivity for hcp Fe, indicating a similar value of the bcc Fe[31] at the ambient pressure condition. The thermal conductivity generally shows a positive pressure dependence for metals,[6] similar to the present results for Pt. Therefore, if the thermal conductivity of the hcp Fe is extrapolated to ambient pressure, it would be smaller than that of the bcc Fe. The small thermal conductivity of the hcp Fe may arise from a low symmetry in the lattice structure of the hcp Fe. As the temperature increases from 300 to 1346 K, the thermal conductivity of the hcp Fe (50–53 GPa) decreases by 32%, which is a similar trend to the bcc Fe.[31] The thermal conductivity of the hcp Fe at higher temperatures is consistent with the reported values obtained from the electrical resistivity[32] and the flash heating method.[20] Further experiments at high pressures and temperatures using the present method would resolve the Earth's core conductivity problem.[20,32]

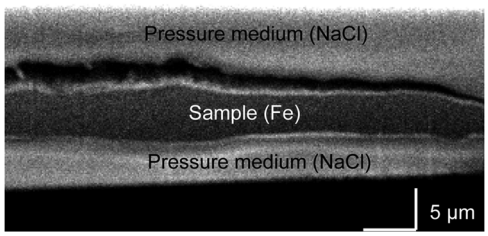

FIG. 6. Cross-sectional SEM image of the Fe sample after the measurement. This image was observed from an oblique angle of 52°. A crack between the Fe and the upper pressure medium formed during the opening process of the DAC.

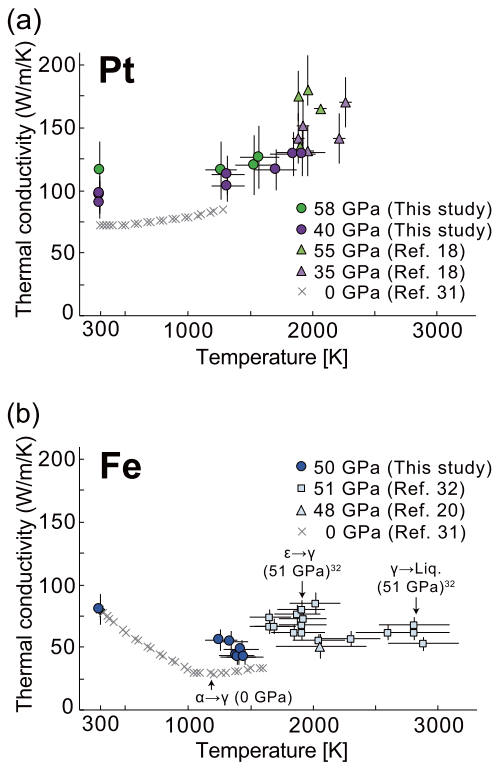

FIG. 7. Temperature dependence of the thermal conductivities of (a) Pt and (b) Fe. Circles indicate results obtained from the thermoreflectance method in this study. Triangles indicate results obtained by the flash heating method by McWilliams *et al.*[18] (Pt) and Konôpková *et al.*[20] (Fe). Squares indicate the calculated data from the electrical resistivity by Ohta *et al.*[32] (Fe). Gray crosses indicate the recommended values at ambient pressure by Ho *et al.*[31] (Pt and Fe). Arrows indicate phase boundaries for Fe. At 51 GPa, Fe undergoes structural phase transitions from ε (hcp) to γ (fcc) at 1900 K and from γ to liquid at 2850 K, respectively.[32] At ambient pressure, the phase transition from α (bcc) to γ in Fe occurs at 1184 K.

B. Uncertainties of the obtained values: Thermal conductivity and temperature

According to Eqs. (1) and (2), the thermal conductivity κ is associated with the heat diffusion time τ, the thickness d, the density ρ, and the isobaric heat capacity C_p of the sample. Therefore, the uncertainties u of each value propagate to that of the thermal conductivity as follows:

$$u_\kappa = \sqrt{\left(\frac{\partial\kappa}{\partial d}\right)^2 u_d^2 + \left(\frac{\partial\kappa}{\partial\tau}\right)^2 u_\tau^2 + \left(\frac{\partial\kappa}{\partial\rho}\right)^2 u_\rho^2 + \left(\frac{\partial\kappa}{\partial C_p}\right)^2 u_{C_p}^2}$$
$$= \sqrt{(2u_d)^2 + (u_\tau)^2 + (u_\rho)^2 + \left(u_{C_p}\right)^2}. \quad (4)$$

The largest uncertainty factor in this study is the thickness of the sample. As shown in the cross-sectional SEM image of the sample (Fig. 6), the disk-shaped sample thickness is not perfectly uniform. The standard deviation of the thickness around the measured position determined from the SEM image is approximately 10%. The uncertainty of the heat diffusion time u_τ was estimated from a fitting error of the transient temperature signals by Eq. (2). The error primarily arose from noise and distortion of the signal, but it did not exceed 5%. For the uncertainty of the density u_ρ, the uncertainty reported in the literature[28,30] was adopted, which was negligible. The values of the heat capacity were derived from the Debye approximation, the validity of which is difficult to examine. Therefore, we did not consider u_{Cp} here. Finally, u_κ is typically 15%.

The uncertainty of the measured temperature of the LHDAC system contains two factors. One is the uncertainty related to the thermal radiation measurement u_{rad}, and the other is related to the heterogeneity of the sample temperature $u_{\Delta T}$ at the CW laser heating caused by the Gaussian shape of the laser energy distribution and the heat dissipation from the sample to the surrounding pressure medium. We concluded that the combined standard uncertainty u_T of the above factors was approximately 10%, according to the following relation:

$$u_T = \sqrt{u_{\mathrm{rad}}^2 + u_{\Delta T}^2}. \quad (5)$$

In this study, 10% of u_T was applied to all the measured data. To determine u_{rad}, we first derived the standard deviation of the residuals between the measured radiation spectrum and the best fit curve, as shown in Fig. 4. Within the standard deviation, we considered the maximum distribution of the Planck's law fitting curve as u_{rad}, which was typically 3%–7% on the measured temperatures.

To estimate the heterogeneity of the sample temperature $u_{\Delta T}$ during the LHDAC operation, we simulated a typical temperature distribution for the Fe sample solving the steady state heat equation using a finite element method (FEM, COMSOL Multiphysics). Figure 8(a) shows the sample structure and boundary conditions used for the FEM. The diameter and thickness of the Fe disk were 75 μm and 7 μm, respectively. The Fe disk was surrounded by NaCl, which had a diameter and thickness of 110 μm and 5 μm, respectively. Temperature of the NaCl/diamond interfaces was fixed by 300 K. On the other hand, the interfaces at the NaCl/Re gasket were set as an adiabatic condition. A heat source with Gaussian distribution was supplied at the central axis of the Fe disk from both faces. The $1/e$ radius of the Gaussian heat source was 15 μm. We assumed thermal conductivity of the Fe as 54.1 W/(m K), based on our measurement result at 53 GPa and 1346 K. For the NaCl, we estimated the thermal conductivity of a B2 phase (high pressure phase of NaCl beyond 27 GPa[34]) between 1000 and 1450 K, which roughly includes a peak temperature and certain temperature decay from the heated spot. For the estimation, we used the equation of state for the B2 NaCl[35] and Leibfried-Schlomann[36] theory as follows:

$$\kappa = \kappa_0 \left(\frac{\rho}{\rho_0}\right)^g \left(\frac{T_0}{T}\right)^m, \quad (6)$$

where κ_0 is 5.7 W/(m K) derived from 18 W/(m K) at 29.2 GPa and 300 K, $g = 2.9$, and $m = 1.0$, according to McGuire *et al.*[37] We obtained 8.0 and 5.5 W/(m K) for the B2 phase from 1000 to 1450 K, respectively. Finally, averaging those values, we imputed 6.8 W/(m K) for the B2 phase into the FEM calculation.

Figure 8(b) shows simulated temperature distribution inside the Fe disk along with the z axis. At the surface irradiated by the CW laser, the temperature shows the highest value and then decreases toward the inside of the Fe disk. The difference in temperature

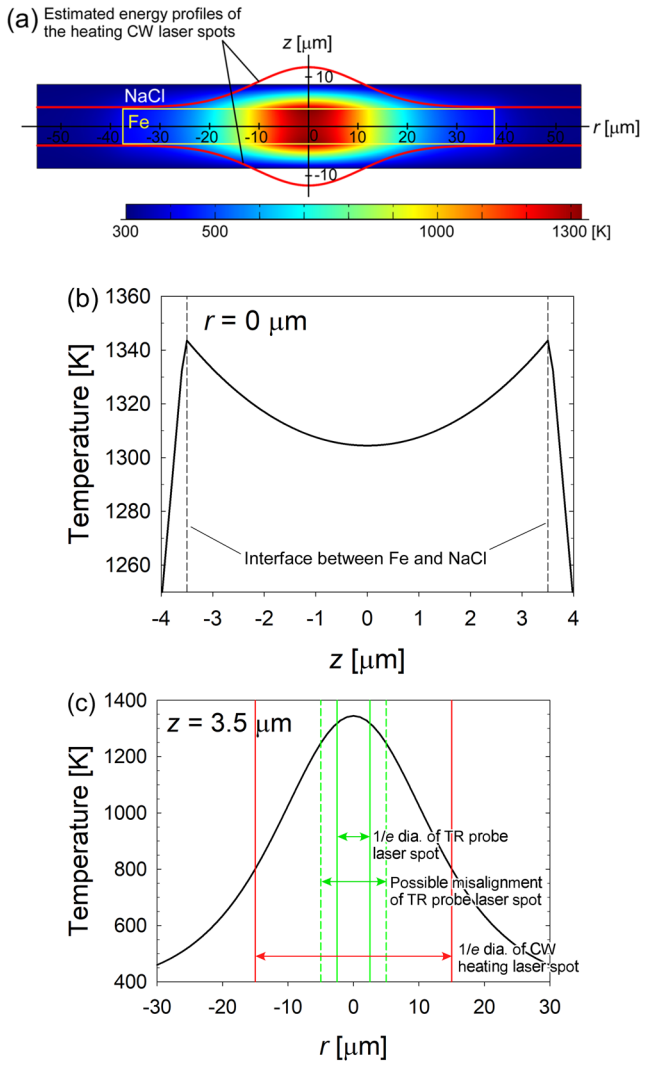

FIG. 8. (a) Simulated temperature distribution of the Fe sample at 53 GPa and 1346 K during LHDAC operation calculated by the finite element method. (b) Cross-sectional temperature distribution inside the Fe disk along the central axis. The temperature gradient in the axial direction is about 3%. (c) Surface temperature of the Fe disk along the radial direction. The vertical lines represent 1/*e* of the diameter of the CW heating laser spot (30 μm), that of the TR probe laser spot (5 μm), and a possible misalignment of the TR probe laser spot (10 μm). The temperature gradient within 10 μm from the center of the CW laser spot is about 7%.

between the surface and the center is about 40 K, which corresponds to 3% of the measured temperature. Figure 8(c) shows the surface temperature of the Fe disk along the radial direction. There is a huge temperature gradient in the radial direction. However, the diameter of the TR probe laser spot is less than 5 μm, and within the spot area, the temperature gradient is negligibly small. Finally, the effect of the temperature gradient in the radial direction was considered to be approximately 7% of the measured temperature, assuming that the misalignment of the TR probe laser was twice its diameter. According to Eq. (4), u_T including the above factors was approximately 10%, which is equal to the temperature uncertainty in the previously reported electrical resistivity[32] and approximately a half of the temperature range in the previously reported flash heating method.[20]

IV. CONCLUSIONS

By combining the TR and LHDAC techniques, we developed an instrument to measure *in situ* high pressure-temperature thermal diffusivity of materials. We determined the thermal conductivities of Pt and Fe using the measured thermal diffusivities up to approximately 60 GPa and 2000 K and obtained values consistent with previous works. The uncertainties in the pressure and the temperature are estimated to be approximately 10%, and that in the thermal conductivity is estimated to be approximately 15%. The system developed in this study enables us to determine thermal transport properties of materials under pressure-temperature conditions present deep in the Earth.

ACKNOWLEDGMENTS

We appreciate Dr. Kuwahara of Advanced Industrial Science and Technology, Japan, for his support in the spectrometer. We are grateful to Professor Hirose of the University of Tokyo for his support in FIB and SEM. This work was supported by JSPS KAKENHI, Grant Nos. JP26247075, 15H05827, and 17H04861.

REFERENCES

[1]T. Lay, J. Hernlund, and B. Buffett, "Core-mantle boundary heat flow," Nat. Geosci. **1**, 25 (2008).
[2]F. Birch and H. Clark, "The thermal conductivity of rocks and its dependence upon temperature and composition," Am. J. Sci. **238**, 529 (1940).
[3]F. Birch and H. Clark, "The thermal conductivity of rocks and its dependence upon temperature and composition. Part II," Am. J. Sci. **238**, 613 (1940).
[4]H. Kanamori, N. Fujii, and H. Mizutani, "Thermal diffusivity measurement of rock-forming minerals from 300° to 1100°K," J. Geophys. Res. **73**, 595, https://doi.org/10.1029/jb073i002p00595 (1968).
[5]K. Horai, "Thermal conductivity of rock-forming minerals," J. Geophys. Res. **76**, 1278, https://doi.org/10.1029/jb076i005p01278 (1971).
[6]R. Ross, P. Anderson, B. Sundqvist, and G. Backstrom, "Thermal conductivity of solids and liquids under pressure," Rep. Prog. Phys. **47**, 1347–1402 (1984).
[7]H. Fujisawa, N. Fujii, H. Mizutani, H. Kanamori, and S. Akimoto, "Thermal diffusivity of Mg_2SiO_4, Fe_2SiO_4, and NaCl at high pressures and temperatures," J. Geophys. Res. **73**, 4727, https://doi.org/10.1029/jb073i014p04727 (1968).
[8]A. E. Beck, D. M. Darbha, and H. H. Schloessin, "Lattice conductivities of single-crystal and polycrystalline materials at mantle pressures and temperatures," Phys. Earth Planet. Inter. **17**, 35 (1978).
[9]T. Katsura, "Thermal diffusivity of periclase at high temperatures and high pressures," Phys. Earth Planet. Inter. **101**, 73 (1997).
[10]Y. Xu, T. Shankland, S. Linhardt, D. Rubie, F. Langenhorst, and K. Klasinski, "Thermal diffusivity and conductivity of olivine, wadsleyite and ringwoodite to 20 GPa and 1373 K," Phys. Earth Planet. Inter. **143**, 321 (2004).
[11]G. M. Manthilake, N. de Koker, and D. J. Frost, "Thermal conductivity of $CaGeO_3$ perovskite at high pressure," Geophys. Res. Lett. **38**, L08301, https://doi.org/10.1029/2011gl046882 (2011).
[12]G. M. Manthilake, N. de Koker, D. J. Frost, and C. A. McCammon, "Lattice thermal conductivity of lower mantle minerals and heat flux from Earth's core," Proc. Natl. Acad. Sci. U. S. A. **108**, 17901 (2011).

[13]M. Osako, E. Ito, and A. Yoneda, "Simultaneous measurements of thermal conductivity and thermal diffusivity for garnet and olivine under high pressure," Phys. Earth Planet. Inter. **143**, 311 (2004).
[14]P. Beck, A. Goncharov, V. Struzhkin, B. Militzer, H. Mao, and R. Hemley, "Measurement of thermal diffusivity at high pressure using a transient heating technique," Appl. Phys. Lett. **91**, 181914 (2007).
[15]A. F. Goncharov, P. Beck, V. Struzhkin, B. Haugen, and S. Jacobsen, "Thermal conductivity of lower-mantle minerals," Phys. Earth Planet. Inter. **174**, 24 (2009).
[16]A. F. Goncharov, V. V. Struzhkin, J. A. Montoya, S. Kharlamova, R. Kundargi, J. Siebert, J. Badro, D. Antonangeli, F. J. Ryerson, and W. Mao, "Effect of composition, structure, and spin state on the thermal conductivity of the Earth's lower mantle," Phys. Earth Planet. Inter. **180**, 148 (2010).
[17]A. F. Goncharov, M. Wong, D. Dalton, J. Ojwang, V. Struzhkin, Z. Konôpková, and P. Lazor, "Thermal conductivity of argon at high pressures and high temperatures," J. Appl. Phys. **111**, 112609 (2012).
[18]R. McWilliams, Z. Konôpková, and A. Goncharov, "A flash heating method for measuring thermal conductivity at high pressure and temperature: Application to Pt," Phys. Earth Planet. Inter. **247**, 17 (2015).
[19]R. McWilliams, D. Dalton, M. Mahmood, and A. Goncharov, "Optical properties of fluid hydrogen at the transition to a conducting state," Phys. Rev. Lett. **116**, 255501 (2016).
[20]Z. Konôpková, R. McWilliams, N. Pérez, and A. Goncharov, "Direct measurement of thermal conductivity in solid iron at planetary core conditions," Nature **534**, 99 (2016).
[21]W.-P. Hsieh, B. Chen, J. Li, P. Keblinski, and D. Cahill, "Pressure tuning of the thermal conductivity of the layered muscovite crystal," Phys. Rev. B **80**, 180302 (2009).
[22]T. Yagi, K. Ohta, K. Kobayashi, N. Taketoshi, K. Hirose, and T. Baba, "Thermal diffusivity measurement in a diamond anvil cell using a light pulse thermoreflectance technique," Meas. Sci. Technol. **22**, 024011 (2011).
[23]K. Ohta, T. Yagi, N. Taketoshi, K. Hirose, T. Komabayashi, T. Baba, Y. Ohishi, and J. Hernlund, "Lattice thermal conductivity of $MgSiO_3$ perovskite and post-perovskite at the core–mantle boundary," Earth Planet. Sci. Lett. **349-350**, 109 (2012).
[24]Y. Okuda, K. Ohta, T. Yagi, R. Sinmyo, T. Wakamatsu, K. Hirose, and Y. Ohishi, "The effect of iron and aluminum incorporation on lattice thermal conductivity of bridgmanite at the Earth's lower mantle," Earth Planet. Sci. Lett. **474**, 25 (2017).
[25]S. Tateno, K. Hirose, Y. Ohishi, and Y. Tatsumi, "The structure of iron in Earth's inner core," Science **330**, 359 (2010).
[26]J. H. Weaver *et al.*, "Thermoreflectance of V, Nb, and paramagnetic Cr," Phys. Rev. B **14**, 459 (1976).
[27]Y. Akahama and H. Kawamura, "High-pressure Raman spectroscopy of diamond anvils to 250 GPa: Method for pressure determination in the multimegabar pressure range," J. Appl. Phys. **96**, 3748 (2004).
[28]M. Matsui, E. Ito, T. Katsura, D. Yamazaki, T. Yoshino, A. Yokoyama, and K. Funakoshi, "The temperature-pressure-volume equation of state of platinum," J. Appl. Phys. **105**, 013505 (2009).
[29]D. Isaak and O. Anderson, "Thermal expansivity of HCP iron at very high pressure and temperature," Physica B **328**, 345 (2003).
[30]D. Yamazaki, E. Ito, T. Yoshino, A. Yoneda, X. Guo, B. Zhang, W. Sun, A. Shimojuku, N. Tsujino, T. Kunimoto, Y. Higo, and K. Funakoshi, "*P-V-T* equation of state for ε-iron up to 80 GPa and 1900 K using the Kawai-type high pressure apparatus equipped with sintered diamond anvils," Geophys. Res. Lett. **39**, L20308, https://doi.org/10.1029/2012gl053540 (2012).
[31]C. Ho, R. Powell, and P. Liley, "Thermal conductivity of the elements," J. Phys. Chem. Ref. Data **1**, 279 (1972).
[32]K. Ohta, Y. Kuwayama, K. Hirose, K. Shimizu, and Y. Ohishi, "Experimental determination of the electrical resistivity of iron at Earth's core conditions," Nature **534**, 95 (2016).
[33]S. Anzellini, A. Dewaele, M. Mezouar, P. Loubeyre, and G. Morard, "Melting of iron at Earth's inner core boundary based on fast x-ray diffraction," Science **340**, 464 (2013).
[34]X. Li and R. Jearoz, "Measurement of the *B*1-*B*2 transition pressure in NaCl at high temperatures," Phys. Rev. B **36**, 474 (1987).
[35]Y. Fei, A. Ricolleau, M. Frank, K. Mibe, G. Shen, and V. Prakapenka, "Toward an internally consistent pressure scale," Proc. Natl. Acad. Sci. U. S. A. **104**, 9182 (2007).
[36]N. de Koker, "Thermal conductivity of MgO periclase at high pressure: Implications for the D″ region," Earth Planet. Sci. Lett. **292**, 392 (2010).
[37]C. McGuire, K. Sawchunk, and A. Kavner, "Measurements of thermal conductivity across the B1-B2 phase transition in NaCl," J. Appl. Phys. **124**, 115902 (2018).